

Core-dominance parameter, black hole mass and jet-disc connection in Fermi blazars

Y.Y. Chen, X. Zhang, H.J. Zhang^{*} and X.L. Yu

Department of physics, Yunnan Normal University, Kunming 650500, China

26 July 2021

ABSTRACT

We study the relationship between jet power and accretion for Fermi and non-Fermi blazars, respectively. We also compare the relevant parameter between them. Our main results are as follows. (i) Fermi and non-Fermi blazars have significant difference in redshift, black hole mass, and broad line luminosity. (ii) Fermi blazars have higher average core-dominance parameter than non-Fermi blazars, which suggests that Fermi blazars have strong beaming effect. (iii) We find significant correlation between broad line emission and jet power for Fermi and non-Fermi blazars, respectively, which suggests a direct tight connection between jet and accretion. (iv) The accretion and black hole mass may have a different contribution to jet power for Fermi and non-Fermi blazars, respectively.

Key words: galaxies: active-galaxies: jets-BL Lacerate objects: general-accretion, accretion discs-radio continue: galaxies-quasars: general

1 INTRODUCTION

Blazars are the most extreme classes of active galactic nuclei (AGN), showing large amplitude and rapid variability, superluminal motion, and strong emission. Blazars also host a jet, pointing almost directly to the observer (Urry & Padovani 1995). Their extreme observation properties can be explained by a beaming effect. Because of a relativistic beaming, the emission that is dominated by a relativistic jet is highly boosted in the line of observer's sight (Urry & Padovani 1995). According to emission line features, blazars are often divided into Flat Spectrum Radio Quasars (FSRQs) and BL Lacerate objects (BL Lacs). Some blazars with an equivalent width (EW) of the emission lines in the rest frame $EW > 5$ are classified as FSRQs (e.g., Scarpa & Falomo 1997; Urry & Padovani 1995). However, Ghisellini et al. (2011) have suggested that this classification is not reliable, and more over does not reflect any intrinsic property or difference within the blazars class. Therefore they introduced a more physical classification based on the luminosity of the broad emission lines measured in Eddington units, and the divided line is of the order of $L_{BLR}/L_{Edd} \sim 5 \times 10^{-4}$. Sbarrato et al. (2012) and Xiong et al. (2014) have confirmed this result. Giommi et al. (2012, 2013) have also deeply investigated the unreliability of the EW classification. They suggested that blazars should be divided into high- and low-ionization sources. Landt et al. (2004) have also introduced

an analogous classification criterion. They found that it is possible to discriminate between objects with intrinsically weak or strong narrow emission lines by studying the $[O_{II}]$ and $[O_{III}]$ EW plane.

Since the launch of the Fermi satellite, we have entered in a new era of blazars research (Abdo et al. 2009, 2010). Up to now, the Large Area Telescope (LAT) has detected hundreds of blazars because it has about 20 folds better sensitivity than its predecessor EGRET in the 0.1-100 GeV energy range. However, at present, there is outstanding question about the AGN, which is unclear that "why are some sources γ -ray loud and others are γ -ray quiet?". Many answers have been proposed to explain this question, such as Doppler boosting, apparent jet speed, apparent opening angle, VLBI core flux densities and brightness temperatures. Blazars detected by LAT are more likely to have higher Doppler factors (e.g., Lister et al. 2009; Savolainen et al. 2010; Tornikoski et al. 2010) and larger apparent opening angles (e.g., Pushkarev et al. 2009) than those not detected by LAT. Many authors have suggested a close connection between the γ -ray emission and radio properties of AGN. Kovalev et al. (2009) have suggested that LAT-detected blazars are brighter and more luminous in the radio domain at parsec scales. Lister et al. (2009) also suggested that LAT-detected blazars have high apparent jet speeds. Pushkarev et al. (2012) also showed that the Fermi AGNs have higher VLBI core flux densities and brightness temperatures. Ghisellini et al. (2010) studied the general physical properties of bright Fermi blazars. According to the SEDs,

* E-mail:kmzhanghj@163.com

they got the jet power and disk luminosity. They found a positive correlation between jet power and the luminosity of the accretion disc in those blazars. Xiong and Zhang (2014) also studied the physical properties of Fermi blazars. Sbarato et al. (2014) found a positive relation between radio luminosity and broad line luminosity in AGNs. However, it is unclear whether there is difference in jet and accretion for LAT blazars and non-LAT blazars. Therefore, we tried to study this question.

In this paper, we collect a large sample of LAT-detected and non-LAT detected blazars, and study the properties of Fermi blazars. The main results of our analysis concern the relation between the jet power and accretion, the relation between jet power and black hole mass in Fermi and no-Fermi blazars, respectively. The paper is structured as follows: we present the sample in Sect.2; the results are in Sect.3; the discussions in Sect.4; the conclusions are in Sect.5. A Λ CDM cosmology with $H_0 = 70 \text{Kms}^{-1}\text{Mpc}^{-1}$, $\Omega_m = 0.27$, $\Omega_\Lambda = 0.73$ is adopted. The energy spectral index α is defined such that $S_\nu \propto \nu^{-\alpha}$

2 THE SAMPLE

The major selection criteria for the sample that we tried to use radio catalogues to get the widest possible sample of blazars from their radio properties, and then split them into Fermi detected sources and non-Fermi detections. Massaro et al.(2009) have described “Multifrequency Catalogue of BLAZARS”, also named Roma-BZCAT. The Roma-BZCAT contains the lists of blazars, which are classified in three main groups based on their spectral properties. Each blazar is identified by a three-letter code. The codes are respectively BZB: BL Lac objects, used for AGNs with a featureless optical spectrum or only with absorption lines of galaxian origin and weak and narrow emission lines; BZQ: flat-spectrum radio quasars, with an optical spectrum showing broad emission lines and dominant blazar characteristics; BZU: blazars of uncertain type, adopted for sources with peculiar characteristics but also showing blazar activity. The widest possible sample of blazars also were included in BZCAT (Massaro et al.2009: The Roma BZCAT) and have reliable radio core and extended luminosity at 1.4 GHz, redshift, black hole mass and broad line luminosity (used as a tracer of the accretion).

Firstly, we consider the following samples of blazars to get the radio core and extended luminosity at 1.4 GHz: Kharb et al. (2010), Antonucci & Ulvestad (1985), Cassaro et al. (1999), Murphy et al. (1993), Landt et al. (2008), Caccianiga et al. (2004), Giroletti et al. (2004). Secondly, we consider the following samples of blazars to get the broad line data: Celotti et al. (1997), Cao & Jiang (1999), Wang et al. (2002, 2004), Liu et al. (2006), Xie et al. (2007), Sbarato et al. (2012), Chai et al. (2012), Shen et al. (2011), Shaw et al. (2012). Thirdly, we consider the following samples of blazars to get black hole mass: Woo & Urry (2002), Cao et al. (2002), D’Elia et al. (2003), Liang & Liu (2003), Xie et al. (2004), Liu et al. (2006), Fan et al. (2008), Zhou & Cao (2009), Xu et al. (2009), Wu et al. (2008), Ghisellini et al. (2011), Zhang et al. (2012), Sbarato et al. (2012), Chai et al. (2012), Leon-Tavares et al. (2011a), Shen et al. (2011), Shaw et al. (2012). At last, we cross-correlated these sample with clean blazars detected by Fermi LAT in two years

of scientific operation (Abdo et al. 2012, 2FGL; Ackermann et al. 2011a, 2LAC). In total, we have a sample containing 177 clean Fermi blazars (96 Fermi FSRQs and 81 Fermi BL Lacs) and 133 non Fermi blazars (105 non-Fermi FSRQs and 28 non-Fermi BL Lacs).

We also note that there may have a select bias about our samples, because our samples only contain the 2LAC clean Fermi blazars and non-EGRET detected blazars in our non-Fermi blazars sample. And all blazars are BZQ or BZB in our sample. The BZU is not contained in our sample. But we find that the redshift distributions of our sample are agree with the Rom-BZCAT. Therefore the select bias should not have large influence for our main results in a certain extent. Xiong and Zhang (2014) have described in detail the calculation of black hole mass and broad line luminosity. In order to reduce the uncertainty, we tried to select the data from a same paper and /or a uniform method as soon as possible. Tremaine et al. (2002) have suggested that the uncertainty in the $M_{\text{BH}} - \sigma$ relation is small, ≤ 0.21 dex; and the uncertainty on the zero point of the line width-luminosity-mass relation is approximately 0.5 dex (Gebhardt et al. 2000; Ferrarese et al. 2001); MuLure & Dunlop (2001) have suggested that the $M_{\text{BH}} - M_R$ correlation for quasars host galaxies has an uncertainty of 0.6 dex (Wang et al. 2004). According to set the Ly α flux contribution to 100, and the relative weights of the H α , H β , MgII and CIV lines to 77, 22, 34 and 63, respectively (see Francis et al. 1991), Celotti, Padovani, & Ghisellini (1997) have calculated the broad line luminosities. We follow Celotti, Padovani, & Ghisellini (1997) and calculate the broad line luminosity for our sample. When more than one line is presented, we calculate the simple average of broad line luminosity estimated from each line. We assume that the uncertainty of broad line luminosity is 0.5dex. Analogously, when more than one black hole mass is gotten, we calculate average black hole mass.

The core-dominance parameter that the ratio of the beamed radio core flux density (S_{core}) to the unbeamed extend radio flux density (S_{ext}) has routinely been used as a statistical indicator of Doppler beaming and orientation (Orr & Browne 1982; Kapahi & Saikia 1982; Kharb & Shastri 2004). We have made a K-correction for the observed flux by using $S(\nu) = S_\nu^{\text{ob}}(1+z)^{\alpha-1}$. The luminosity is calculated from the relation $L_\nu = 4\pi d_L^2 S_\nu$. We calculate the core-dominance parameter ($R_c = \frac{S_{\text{core}}}{S_{\text{ext}}}(1+z)^{\alpha_{\text{core}}-\alpha_{\text{ext}}}$, with $\alpha_{\text{core}} = 0$, $\alpha_{\text{ext}} = 0.8$)

The jet power also can be derived from the lobe low frequency radio emission under the assumption of minimum energy arguments(e.g., Rawlings & Saunders 1991; Willott et al. 1999). This approach now is widely used to estimate the jet kinetic energy in AGNs. Meyer et al.(2011) used the following formula to estimated the cavity kinetic power,i.e.,

$$\log P_{\text{cav}} = 0.64(\pm 0.09)(\log L_{300} - 40) + 43.54(\pm 0.12) \quad (1)$$

where L_{300} is the extend luminosity at 300 MHz, the unit of jet power is erg s^{-1} , which is continuous over $\sim 6-8$ decades in P_{jet} and P_{radio} with a scatter of $\sim 0.7\text{dex}$ and $P_{\text{cav}} = P_{\text{jet}}$. We extrapolate the extend 1.4 GHz flux density to calculate the extend 300 MHz flux density, by assuming a spectral index of $\alpha = 1.2$ in this paper. We use equation (1) to get the jet power.

The relevant data for Fermi blazars is listed in Table 2 with the following headings: column (1) the name of the

Fermi blazars (2FGL); column (2) classification of *Fermi* blazars (BZQ=FSRQ, BZB=BL Lac); column (3) the redshift; column (4) the radio core flux density at 1.4 GHz, the units is Jy; column (5) the radio extended flux density at 1.4 GHz, the units is mJy; column (6) the references of column (4) and column (5); column (7) the black hole mass; column (8) the references of the black hole mass; column (9) the broad line luminosity, the units is ergs^{-1} ; column (10) the references of broad line luminosity. The relevant data for non-*Fermi* blazars is also listed in Table 3.

3 RESULTS

3.1 The distributions

We make the histogram about redshift for the various classes in Figs. 1. From Fig.2 of Rom-BZCAT, the redshift distributions of BL Lacs are much closer than that of FSRQs and their distribution peaks at $z \approx 0.3$, whereas FSRQs show a broad maximum between 0.6 and 1.5. There are only very few BL Lacs at redshift higher than 0.8. So our results agree with the results of Rom-BZCAT in the redshift distributions. From Figs.1, we can see that the range of redshift is $0 < z < 2.5$ and $0 < z < 3.5$ for *Fermi* and non-*Fermi* blazars. The mean redshift are listed in Table 1. Through nonparametric Kolmogorov-Smirnov (K-S) test, we get that the distributions of redshift between all *Fermi* blazars and all non-*Fermi* blazars, between *Fermi* FSRQs and non-*Fermi* FSRQs are significantly different (see Table 1, significant probability $P < 0.05$). However, there is no significant difference between *Fermi* BL Lacs and non-*Fermi* BL Lacs. The non-*Fermi* FSRQs have higher average redshift than *Fermi* FSRQs. The *Fermi* BL Lacs have higher average redshift than non-*Fermi* BL Lacs. Linford et al. (2011) suggested that it is still enough to rule out redshift as the cause of LAT non-detection. If assuming the non-LAT BL Lacs might have been too far away to detect their γ -rays. We find that the LAT BL Lacs have higher average redshift than non-LAT BL Lacs. Therefore we confirm the result of Linford et al. (2011). They also found that there is no strong correlation between redshift and γ -ray flux for the BL Lac objects.

The black hole mass distributions of the various classes are shown in Figs. 2. The mean black hole mass are listed in Table 1 for various classes. Through the K-S test, we get that the distributions of black hole mass between all *Fermi* blazars and all non-*Fermi* blazars, between *Fermi* FSRQs and non-*Fermi* FSRQs are significantly different. However, there is no significant difference between *Fermi* BL Lacs and non-*Fermi* BL Lacs (see Table 1). Compared with *Fermi* FSRQs, the non-*Fermi* FSRQs have higher mean black hole mass. Compared with the *Fermi* BL Lacs, the non-*Fermi* BL Lacs have higher mean black hole mass. There may be a general think that the *Fermi* blazars may have large black hole mass (Ghisellini et al. 2010). We should notice that the γ -ray narrow line Seyfert 1 have lower black hole mass than blazars, whereas it can be detected by LAT. Meier (1999) have suggested that it is not necessary to have a relatively massive black hole to produce powerful jet. According to the current accretion and jet production theory (Blandford & Znajek 1977; Meier 1999; Xie et al. 2006, 2007; Chai et al. 2012), jet power is linked with the spinning of black hole.

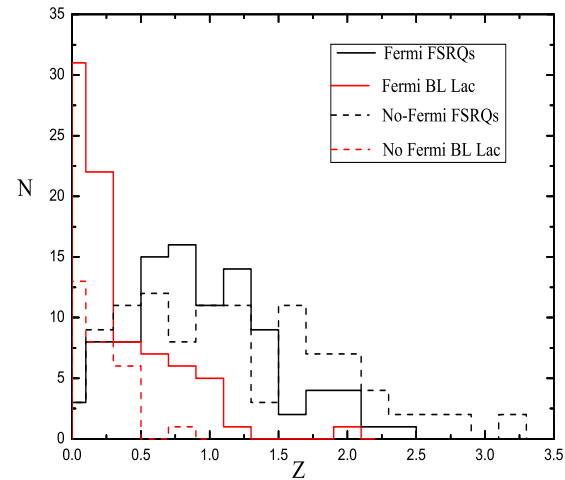


Figure 1. Distributions of redshifts of *Fermi* and non-*Fermi* blazars. The black solid line is *Fermi* FSRQs. The red solid line is *Fermi* BL Lac. The black dashed line is non-*Fermi* FSRQs. The red dashed line is non-*Fermi* BL Lac.

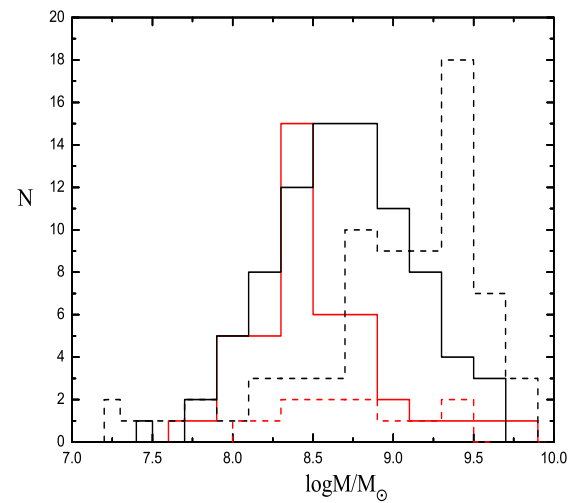
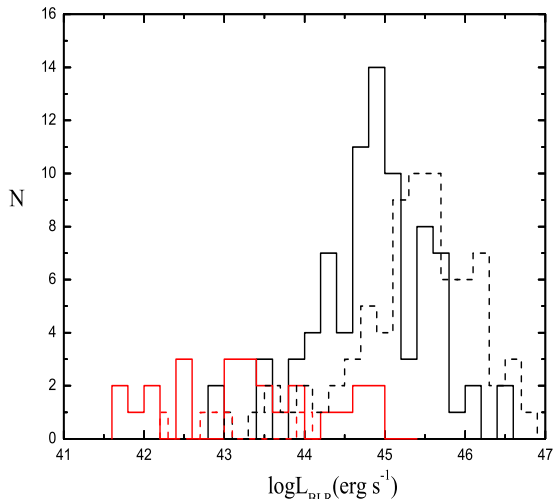


Figure 2. Distributions of black hole mass of *Fermi* and non-*Fermi* blazars. The meanings of different lines are as same as Fig.1.

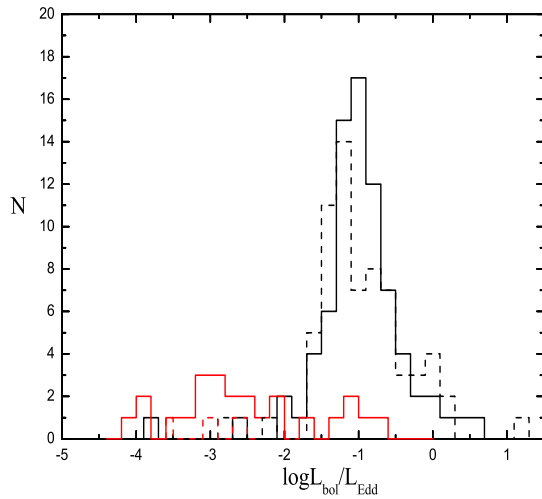
The broad line luminosity distributions for the various classes are shown in Figs. 3. The mean broad line luminosity are listed in Table 1 for various classes. Through the K-S test, we get that the broad line luminosity distributions between all *Fermi* blazars and non-*Fermi* blazars, between *Fermi* FSRQs and non-*Fermi* FSRQs are significantly different (see Table 1). Compared with *Fermi* FSRQs, the non-*Fermi* FSRQs have higher mean broad line luminosity. The Eddington ratio distributions for the various classes are shown in Figs. 4 ($L_{\text{bol}}/L_{\text{Edd}}$, $L_{\text{bol}} \approx 10L_{\text{BLR}}$,

Table 1. The KS test on properties of Fermi and non-Fermi blazars.

Parameter	probability	Significantly different	subsets	mean(Fermi)	mean(non-Fermi)
z	0.002	YES	allblazars	0.74 ± 0.56	1.06 ± 0.79
	0.011	YES	FSRQs	1.03 ± 0.52	1.27 ± 0.75
	0.249	NO	BL	0.40 ± 0.37	0.28 ± 0.19
$\log(M/M_{\odot})$	2.36×10^{-6}	YES	allblazars	8.72 ± 0.44	9.03 ± 0.59
	3.28×10^{-5}	YES	FSRQs	8.78 ± 0.43	9.07 ± 0.61
	0.408	NO	BL	8.61 ± 0.43	8.81 ± 0.43
$\log L_{\text{BLR}}$	1.56×10^{-7}	YES	allblazars	44.60 ± 1.03	45.33 ± 0.94
	1.5×10^{-5}	YES	FSRQs	44.97 ± 0.70	45.44 ± 0.79
	0.084	NO	allblazars	-1.26 ± 0.96	-0.93 ± 0.73
$\log L_{\text{bol}}/L_{\text{Edd}}$	0.408	NO	FSRQs	-0.90 ± 0.60	-0.84 ± 0.60
	0.435	NO	allblazars	42.59 ± 1.36	42.71 ± 1.27
	0.001	YES	FSRQs	43.67 ± 0.58	43.20 ± 0.88
$\log L_{\text{core}}$	0.071	NO	BL	41.60 ± 1.09	40.98 ± 0.84
	0.086	NO	allblazars	41.52 ± 1.30	41.65 ± 1.15
	2.75×10^{-4}	YES	FSRQs	42.50 ± 0.76	41.98 ± 0.99
$\log R_c$	0.672	NO	BL	40.71 ± 1.08	40.51 ± 0.92
	0.50	NO	allblazars	1.10 ± 0.68	1.04 ± 0.81
	0.952	NO	FSRQs	1.18 ± 0.57	1.22 ± 0.73
	0.004	YES	BL	1.03 ± 0.77	0.40 ± 0.79

**Figure 3.** Distributions of broad line luminosity of Fermi and non-Fermi blazars. The meanings of different lines are as same as Fig.1.

$L_{\text{Edd}}=1.3 \times 10^{38} (M/M_{\odot}) \text{ ergs}^{-1}$. The mean Eddington ratios are also listed in Table 1. Through the K-S test, we get that the Eddington ratio distributions between all Fermi blazars and non-Fermi blazars, between Fermi FSRQs and non-Fermi FSRQs have no significant difference (see Table 1). Compared with Fermi FSRQs, the non-Fermi FSRQs have higher mean Eddington ratios. Due to few non-Fermi BL Lacs having broad line luminosity, we only compare broad line luminosity distributions between Fermi FSRQs and non-Fermi FSRQs. Ghisellini et al. (1998) have suggested that the difference between the jet production mechanisms may also manifest in the observed luminosity, which has been proposed to unify the subclasses of blazars as a

**Figure 4.** Distributions of Eddington ratios of Fermi and non-Fermi blazars. The meanings of different lines are as same as Fig.1.

blazar sequence. Ghisellini et al. (2009a, 2010) have suggested that the difference between BL Lacs and FSRQs may be associated with the different accretion rate, because of a very weak BLR may form if the accretion rate is low than $10^{-2} L_{\text{Edd}}$ (Ho 2008). Therefore, the BLR is also related to the accretion disk structure and the disk radiative efficiency. The division between BL Lacs and FSRQs may be observationally controlled by the luminosity of the BLR measured in Eddington units (Ghisellini et al. 2011; Sbarato et al. 2012; Zhang et al. 2014).

The core luminosity distributions for the various classes are shown in Figs. 5. The mean core luminosities are listed in Table 1 for various classes. Through the K-S test, we get that

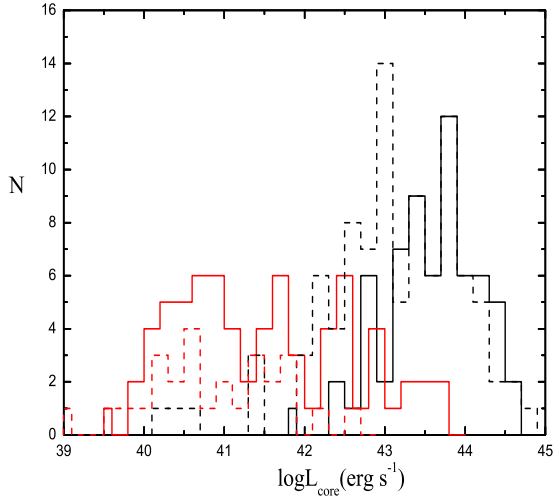


Figure 5. Distributions of core luminosity of Fermi and non-Fermi blazars. The meanings of different lines are as same as Fig.1.

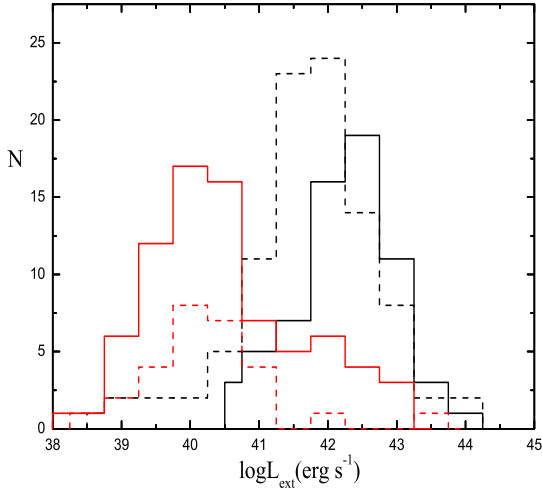


Figure 6. Distributions of extended luminosity of Fermi and non-Fermi blazars. The meanings of different lines are as same as Fig.1.

the core luminosity distributions between all Fermi blazars and all non-Fermi blazars, between Fermi BL Lacs and non-Fermi BL Lacs have no significant difference (see Table 1). However, there is significant difference between Fermi FSRQs and non-Fermi FSRQs. The Fermi FSRQs have higher mean core luminosity than non-Fermi FSRQs. The Fermi BL Lacs have higher mean core luminosity than non-Fermi BL Lacs.

The extended radio luminosity distributions for the various classes are shown in Figs. 6. The mean extended radio luminosities are listed in Table 1 for various classes. Through the K-S test, we get that the extended radio luminosity be-

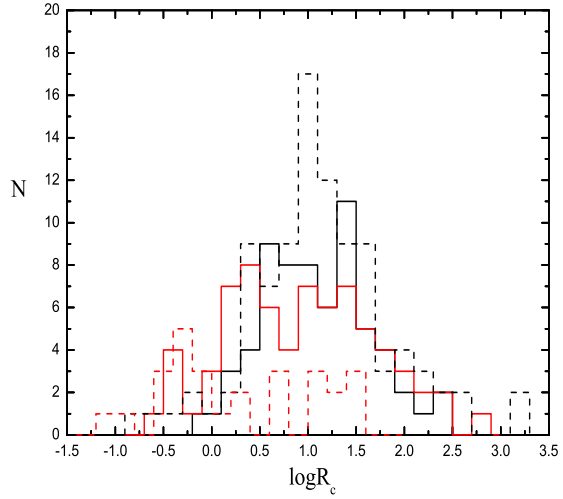


Figure 7. Distributions of core-dominance parameter of Fermi and non-Fermi blazars. The meanings of different lines are as same as Fig.1.

tween all Fermi blazars and all non-Fermi blazars, between Fermi BL Lacs and non-Fermi BL Lacs have no significant difference. However, there is significant difference between Fermi FSRQs and non-Fermi FSRQs (see Table 1). The extend radio luminosity can be used to indicate the intrinsic jet power. This result may suggest that there have no significant different in intrinsic jet power for all Fermi and all non-Fermi blazars. Compared with Fermi FSRQs, the non-Fermi FSRQs have lower average extended radio luminosity. Compared with non-Fermi BL Lacs, the Fermi BL Lacs have higher average extended radio luminosity.

The core-dominance parameter distributions for the various classes are shown in Figs.7. The range of core-dominance parameter is from $10^{-0.75}$ to $10^{3.0}$ for all Fermi blazars; the scope of core-dominance parameter is from $10^{-1.25}$ to $10^{3.50}$ for all non-Fermi blazars. The average core-dominance parameters are listed in Table 1 for various classes. Through the K-S test, we get that the distributions between all Fermi blazars and all non-Fermi blazars, between Fermi FSRQs and non-Fermi FSRQs have no significant difference. However, there is significant difference between Fermi BL Lacs and non-Fermi BL Lacs (see Table 1). Compared with all non-Fermi blazars, the all Fermi blazars have higher average core-dominance parameter, which suggests that the Fermi blazars have strong beaming effect. The Fermi FSRQs have lower average core-dominance parameter than non-Fermi FSRQs. The Fermi BL Lacs have significantly higher average core-dominance parameter than non-Fermi BL Lacs. Kharb et al. (2010) found that the ratio of the radio core luminosity to the k-corrected optical luminosity ($\log R_\nu = \log \frac{L_{\text{core}}}{L_{\text{opt}}} = (\log L_{\text{core}} + M_{\text{abs}}/2.5) - 13.7$) appears to be a better indicator of orientation than traditionally used radio core-dominance parameter (R_c). They suggested that the extended radio luminosity may be affected by interaction with the environment on Kiloparsec-scales. We find that there is no significant difference between Fermi and

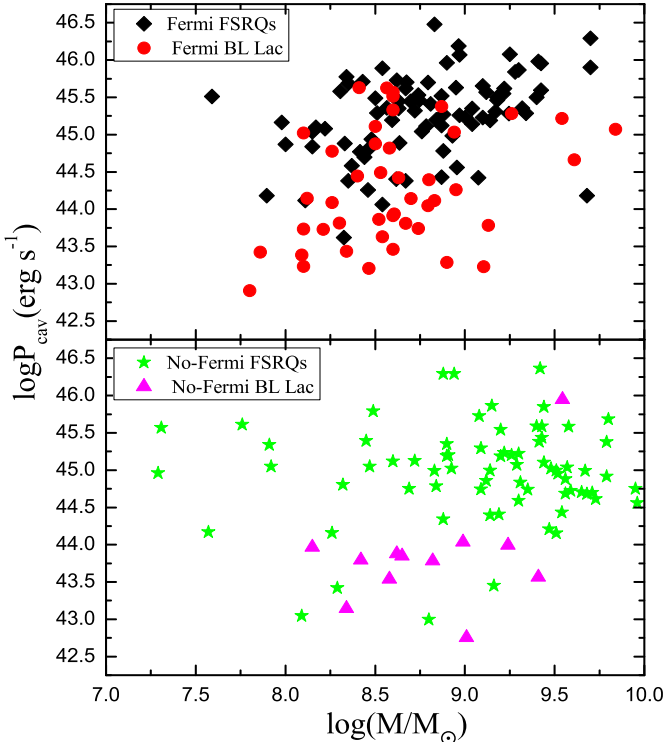


Figure 8. The jet power as a function of black hole mass for Fermi (top) and non-Fermi blazars (bottom). The black square is Fermi FSRQs . The filled red circle is Fermi BL Lacs. The green stars is non-Fermi FSRQs. The magenta triangles is non-Fermi BL Lacs.

non-Fermi FSRQs in the distributions of core-dominance parameter. Because of the FSRQs have a rich dense environment, which may lead to above result that the distributions difference of core-dominance parameter between Fermi and non-Fermi FSRQs.

3.2 Jet power vs black hole mass and Eddington ratio

The relationship between jet power and black hole mass is shown in Figs.8. Different symbols correspond to blazars of different classes. We use the Pearson's analysis to analyze the correlations between jet power and black hole mass for all blazars (Ackermann et al. 2011b; Padovani 1992; Machalski & Jamrozy 2006). We find significant correlations between jet power and black hole mass for Fermi blazars (number of points $N=129$, significance level $P<0.0001$, coefficient of correlation $r=0.40$). However, there have no significant correlations for non-Fermi blazar($N=84$, $P=0.11$, $r=0.18$). Figs.9 shows the relationship between jet power and Eddington ratio. We also find that there are significant correlations between jet power and Eddington ratio for both Fermi blazars and non-Fermi blazars (Fermi blazars: $N=101$,

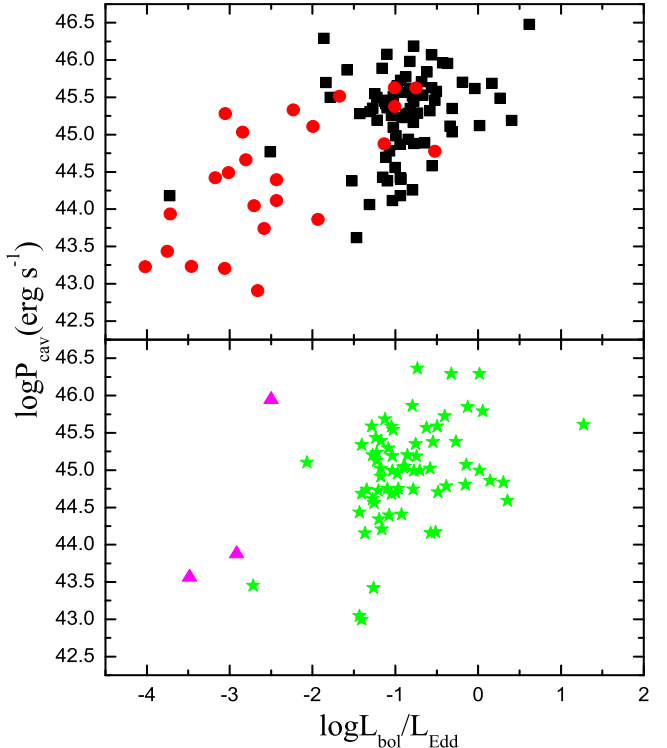


Figure 9. The jet power as a function of Eddington ratio of Fermi (top) and non-Fermi (bottom) blazars. The meanings of different symbols are as same as Fig.8.

$P<0.0001$, $r=0.63$; non-Fermi blazars: $N=70$, $P<0.0001$, $r=0.42$).

3.3 Broad line luminosity vs jet power

The luminosity in the BLR can be taken as an indication of the accretion power of the source (Celotti et al. 1997). We also present a correlation between the broad line emission and jet power for our sample of blazars. Figure 10 and 11 show the broad line luminosity as a function of jet power for Fermi blazars and non-Fermi blazars, respectively. The results of Pearson's analysis show that there are significant correlations between broad line luminosity and jet power for both Fermi blazars and non-Fermi blazars (Fermi blazars: $N=76$, $P<0.0001$, $r=0.74$; non-Fermi blazars: $N=72$, $P<0.0001$, $r=0.41$). We use a linear regression to analyze the correlation between broad line luminosity and jet power. We obtain $\log L_{\text{BLR}} \sim (1.06 \pm 0.11) \log P_{\text{cav}}$ for Fermi blazars; $\log L_{\text{BLR}} \sim (0.59 \pm 0.16) \log P_{\text{cav}}$ for non-Fermi blazars (95% confidence level).

It is generally believed that the jet formation occurs via either BZ (Blandford & Znajek 1977) mechanisms and /or either the BP (Blandford & Payne 1982). AGN jet may be driven by both the accretion process and the spin of central BH (Fanidakis et al. 2011; Zhang et al. 2012,2014). Davis &

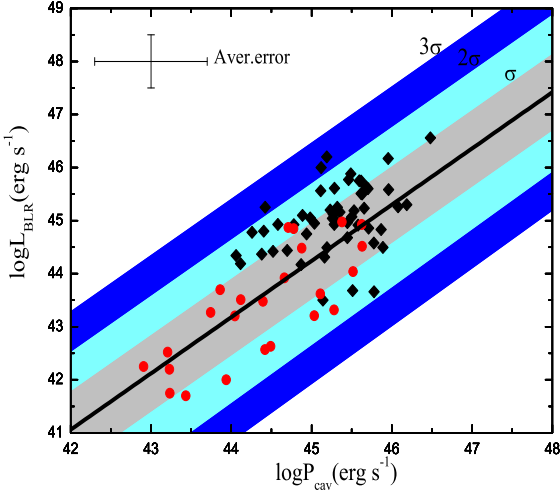


Figure 10. The broad line luminosity as a function of jet power of *Fermi* blazars. Shaded colored areas correspond to 1, 2 and 3 σ (vertical) dispersion, $\sigma = 0.74$. The black line is the best least square fit ($\log L_{\text{BLR}} = 1.06 \log P_{\text{cav}} - 3.46$). The average error bar corresponds to an uncertainty of a factor 0.5 in $\log L_{\text{BLR}}$ and 0.7 in $\log P_{\text{cav}}$. The meanings of different symbols are as same as Fig.8.

Laor (2011) suggested that the BH mass would be also an essential factor for the jet radiation efficiency and jet power. The different relationship between jet power and both accretion and black hole mass may indicate the different dominating jet formation mechanisms. We further investigate the connection between the jet properties and both the accretion and central BH. We use multiple linear regression analysis to get the relationships between jet power and both the Eddington luminosity and the broad line region luminosity for *Fermi* and non-*Fermi* blazars with 95% confidence level and $r=0.77, 0.44$ (Figs. 12);

$$\log P_{\text{cav}} = 0.52(\pm 0.06) \log L_{\text{BLR}} + 0.09(\pm 0.15) \log L_{\text{Edd}} + 17.56(\pm 6.73), \quad (2)$$

$$\log P_{\text{cav}} = 0.39(\pm 0.11) \log L_{\text{BLR}} - 0.14(\pm 0.16) \log L_{\text{Edd}} + 33.72(\pm 6.72). \quad (3)$$

From Equations (2) and (3), we see that both accretion and black hole mass have contributions to the jet power for non-*Fermi* blazars. However, the black hole mass does not have significant influence on jet power for *Fermi* blazars. Ghisellini et al.(2014) have suggested that the jet power may depend on the spinning of black hole but the accretion for *Fermi* blazars.

4 DISCUSSIONS AND CONCLUSIONS

In this paper, we study the difference between *Fermi* and non-*Fermi* blazars by using a large sample. Our results are as follows:(i) Compared with non-*Fermi* blazars, the *Fermi* blazars have lower redshift, lower black hole mass,

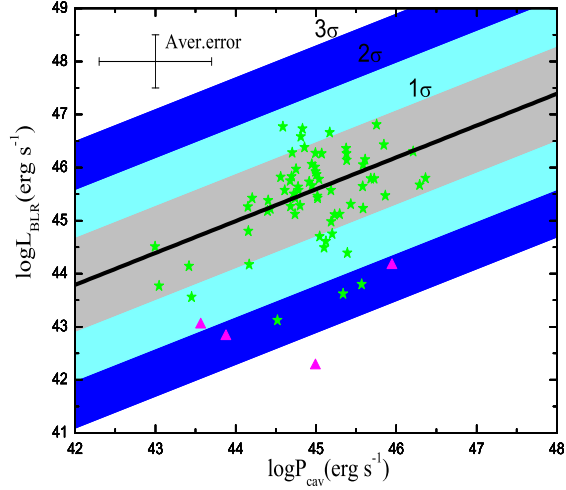


Figure 11. The broad line luminosity as a function of jet power of non-*Fermi* blazars. Shaded colored areas correspond to 1, 2 and 3 σ (vertical) dispersion, $\sigma = 0.90$. The black line is the best least square fit ($\log L_{\text{BLR}} = 0.59 \log P_{\text{cav}} + 18.59$). The meanings of different symbols are as same as Fig.8.

lower broad line luminosity, lower core luminosity and lower extended luminosity on the average. However, the *Fermi* blazars have higher average core-dominance parameter than non-*Fermi* blazars. (ii) Generally, the extend radio luminosity can be used to indicate the intrinsic jet power. The core-dominance parameter can be used as a indicator of beaming effect. The *Fermi* and non-*Fermi* blazars could have differences either in intrinsic jet power, or in inclination angle with respect to the beamed jet emission. However, we find that there have no significant difference in intrinsic jet power for all *Fermi* and all non-*Fermi* blazars. This result may be explained as follows: Kharb et al.(2010) have suggested that the extend radio luminosity could be affected by interaction with the environment on kiloparsec-scales. The optical luminosity is likely to be a better measure of intrinsic jet power than extend radio luminosity (e.g., Maraschi et al.2008; Ghisellini et al.2009). This is due to the fact that the optical continuum luminosity is correlated with the emission-line luminosity over 4 orders of magnitude (Yee & Oke 1978), and the emission-line luminosity is tightly correlated with the total jet kinetic power (Rawlings & Saunders 1991). We also find that there have no significant difference in core-dominance parameter (inclination angle) for all *Fermi* and all non-*Fermi* blazars. This result may be explained as follows: Kharb et al. (2010) found that the ratio of the radio core luminosity to the k-corrected optical luminosity ($\log R_\nu = \log \frac{L_{\text{core}}}{L_{\text{opt}}} = (\log L_{\text{core}} + M_{\text{abs}}/2.5) - 13.7$) appears to be a better indicator of orientation than traditionally used radio core-dominance parameter (R_c).

Compared with *Fermi* FSRQs, the non-*Fermi* FSRQs have significant higher mass, and significant higher accretion luminosity, and significant lower core and lower extend radio emission, but similar accretion luminosity in Eddington units and similar radio core-dominance parameter (which

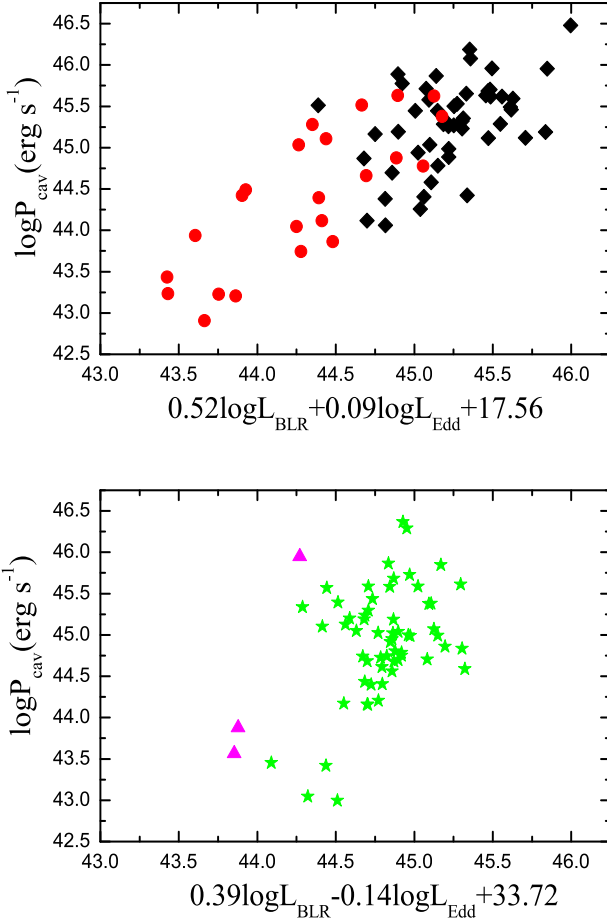


Figure 12. The jet power as a function of both broad line luminosity and Eddington luminosity of Fermi (top) and non-Fermi (bottom) blazars. The meanings of different symbols are as same as Fig.8.

may imply they are seen at similar angles to the jet). However, there is plainly lots of overlap between the Fermi and non-Fermi FSRQs. If using the extend radio luminosity to indicate the intrinsic jet power, the results may suggest that the Fermi FSRQs have stronger jet than non-Fermi FSRQs. There may be a general think that the Fermi blazars may have large black hole mass (Ghisellini et al. 2010). Our results seem to contradict with the idea. Meier (1999) have demonstrated explicitly that it is not necessary to have a relatively massive black hole mass to produce powerful jet. Many authors have suggested that the jet power is tied to the spinning of black hole based on current accretion and jet production theory (e.g., Blandford & Znajek 1977; Meier 1999; Ghisellini et al. 2014). These results suggest that the Fermi FSRQs may have higher spinning than non-Fermi FSRQs. Linford et al.(2012) have suggested that the LAT FS-

RQs had higher radio flux densities than non-LAT FSRQs. Dermer et al.(1995) have suggested that the radio should be beamed in a different way to the Fermi flux in the FSRQs. So the radio should be a broader beam as its seed photons come from the magnetic field which is isotropic in the jet frame. The external compton fermi flux is from seed photons from the BLR which are isotropic in the observer frame and highly anisotropic in the jet frame. The Fermi FSRQ should be those with smaller jet angle (Dermer et al 1995).

Urry & Padovani (1995) have suggested that many of the main properties of blazars can be explained by the relativistic jets. However, jets formation remains one of the unsolved fundamental problems in astrophysics (Meier et al. 2001). Many models have been proposed to explain the origin of the jets. Two basic of theoretical models have been suggested for the origin of jets: (1) If the black hole is spinning rapidly, the rotational energy of the black hole is expected to be transferred to the jets by the magnetic fields threading the holes (Blandford & Znajek 1977), (2) The jet can also be accelerated by the large-scale fields threading the rotating accretion disk (Blandford & Payne 1982). Our results show that there is significant correlation between jet power and black hole mass for Fermi blazars. The Pearson's analysis show that there are significant correlations between jet power and broad line luminosity for both Fermi blazars and non-Fermi blazars, which support that jet power has a close link with accretion. Many authors have confirmed this result (Rawlings & Saunders 1991; Falcke & Biermann 1995; Serjeant et al. 1998; Cao & Jiang 1999; Wang et al. 2004; Liu et al. 2006; Xie et al. 2007; Ghisellini, et al. 2009a, 2009b, 2010, 2011; Gu et al. 2009; Sbarrato et al. 2012). Our results suggest that the jet power depends on both the accretion and black hole mass. A linear regression is applied to analyze the correlation between jet power and broad line luminosity, and we obtain $\log L_{BLR} \sim (1.06 \pm 0.06) \log P_{cav}$ for Fermi blazars; $\log L_{BLR} \sim (0.59 \pm 0.16) \log P_{cav}$ for non-Fermi blazars. Ghisellini et al. (2014) also got a close connection between jet powers and accretion disk luminosity for Fermi blazars. Our result is consistent with them.

Ghisellini (2006) have suggested if relativistic jets are powered by a Poynting flux, the Blandford & Znajek (1997) power can be written as

$$L_{BZ,jet} \sim \left(\frac{\alpha}{m}\right)^2 \frac{R_S^3}{HR^2} \frac{\varepsilon_B}{\eta} \frac{L_{disk}}{\beta_r}. \quad (4)$$

where L_{BZ} is the BZ luminosity; $\frac{\alpha}{m}$ is the specific black hole angular momentum; and B is the magnetic field in gauss; $R_S = 2GM_B/c^2$ is the Schwarzschild radius; R is the radius; and ε_B is the fraction of the available gravitational energy; η is the accretion efficiency (Xie et al. 2007); β_r is the radial inflow velocity and H is the disk thickness. Ghisellini (2006) also suggested that the maximum BZ jet power can be written as

$$L_{jet} \sim \frac{L_{disk}}{\eta}. \quad (5)$$

In addition, in view of current theories of accretion disks, the BLR is ionized by a nuclear source (probably radiation from the disk). Maraschi & Tavecchio (2003) obtained

$$L_{BLR} = \tau L_{disk}, \quad (6)$$

where τ is the fraction of the central emission reprocessed

by the BLR, usually assumed to be 0.1. From equations (5) and (6), we have

$$L_{\text{BLR}} \sim \tau \eta L_{\text{jet}}. \quad (7)$$

From equation (7), we have

$$\log L_{\text{BLR}} = \log L_{\text{jet}} + \log \eta + \text{const.} \quad (8)$$

Equation (8) shows that the theoretical predicted coefficient of the $\log L_{\text{BLR}} - \log L_{\text{jet}}$ relation is 1. From our results, it is seen that the coefficient of $\log L_{\text{BLR}} \sim \log P_{\text{cav}}$ relation for *Fermi* blazars is consistent with the theoretical predicted coefficient while is not for non-*Fermi* blazars.

ACKNOWLEDGMENTS

We sincerely thank the Chris Done for valuable comments and suggestions. We are very grateful to the Science Foundation of Yunnan Province of China(2012FB140,2010CD046). This work is supported by the National Nature Science Foundation of China (11063004,11163007,U1231203), and the High-Energy Astrophysics Science and Technology Innovation Team of Yunnan Higher School and Yunnan Gravitation Theory Innovation Team (2011c1). This research has made use of the NASA/IPAC Extragalactic Database (NED),that is operated by Jet Propulsion Laboratory, California Institute of Technology, under contract with the National Aeronautics and Space Administration.

REFERENCES

- Abdo A. A. et al., 2012, ApJS, 199, 31
 Abdo A. A., Ackermann, M., Ajello, M., et al. 2009, ApJ, 700, 597
 Abdo, A. A., Ackermann, M., Ajello, M., et al. 2010, ApJ, 715, 429
 Ackermann M. et al., 2011a, ApJ, 741, 30
 Ackermann M., Ajello M., Allafort A. et al., 2011b, ApJ, 741, 30
 Antonucci R.R.J., & Ulvestad J.S., 1985, ApJ, 294, 158 (A85)
 Blandford R.D. & Znajek R.L., 1977, MNRAS, 179, 433
 Blandford R.D. & Payne D.G., 1982, MNRAS, 199, 883
 Blandford R.D., & Konigl A., 1979, ApJ, 232, 34
 Caccianiga A., & Marchā M.J.M., 2004, MNRAS, 348, 937 (C04)
 Cao X., & Jiang D. R., 1999, MNRAS, 307, 802 (C99)
 Cao X.W., 2002, ApJ, 570, L13 (C02)
 Cassaro P., Stanghellini C., Bondi M., Dallacasa D., et al. 1999, A&A, 339, 601c (CB99)
 Celotti A., Padovani P., & Ghisellini G., 1997, MNRAS, 286, 415 (C97)
 Chai B., Cao X., & Gu M., 2012, ApJ, 759, 114 (C12)
 Davis, S.W., & Laor, A., 2011, ApJ, 728, 98
 D'Elia V., 2003, MNRAS, 339, 108 (D03)
 Dermer, C.D., 1995, ApJ, 446, L63
 Falcke H. & Biermann P.L., 1995, A&A, 293, 665
 Fan, J. H., Yuan, Y. H., Huang, Y., Gao, Y., Hua, T. X., & Liu, Y., 2008, IAUS, 245, 243 (F08)
 Ferrarese L., et al., 2001, ApJ, 555, L79
 Francis P.J., Hewett P.C., Foltz C.B., Chaffee F.H., Weymann R.J. & Morris S.L., 1991, ApJ, 373, 465
 Fanidakis N., Baugh C. M., Benson A. J., et al., 2011, MNRAS, 410, 53
 Gebhardt K., et al., 2000, ApJ, 543, L5
 Ghisellini, G., Celotti, A., Fossati, G., Maraschi, L., & Comastri, A., 1998, MNRAS, 301, 451
 Ghisellini G., 2006, in Proc. VI Microquasar Workshop: Microquasars and Beyond, http://pos.sissa.it//archive/conferences/033/027/MQW6_027.pdf
 Ghisellini G., Maraschi L. & Tavecchio F., 2009a, MNRAS, 396, 105
 Ghisellini G., Tavecchio F., Foschini L., & Ghirlanda G., 2011, MNRAS, 414, 2674 (G11)
 Ghisellini G., Tavecchio F., Foschini L., Ghirlanda G., Maraschi L. & Celotti A., 2009b, MNRAS, 402, 497
 Ghisellini G., Tavecchio F., Foschini L., Ghirlanda G., Maraschi L. & Celotti A., 2010, MNRAS, 402, 497
 Ghisellini, G.; Tavecchio, F.; Maraschi, L.; Celotti, A.; & Sbarato, T., 2014, Nature, 515, 376
 Giommi P., Padovani P., Polenta G., Turziani S., D'Elia V., & Piranomonte S., 2012, MNRAS, 420, 2899
 Giommi P., Padovani P., & Polenta G., 2013, MNRAS, 431, 1914
 Giroletti M., & Giovannini G., 2004, ApJ, 613, 752 (GM04)
 Gu M., Cao X., & Jiang D.R., 2009, MNRAS, 396, 984
 Ho, L. C., 2008, ARA&A, 46, 475
 Kapahi, V. K., & Saikia, D. J. 1982, JA&A, 3, 465
 Kharb P., Lister M.L., & Cooper N.J., 2010, ApJ, 710, 764 (K10)
 Kharb, P., & Shastri, P. 2004, A&A, 425, 825
 Landt H., & Bignall H.E., 2008, MNRAS, 391, 967 (L08)
 Landt H., Padovani P., Giommi P., & Perlman E. S., 2004, MNRAS, 351, 83
 Leon-Tavares J., Valtaoja E., Chavushyan V. H., Tornikoski M., Añorve C., Nieppola E., & Lähteenmäki A., 2011a, MNRAS, 411, 1127 (L11)
 Liang E.W., & Liu H.T., 2003, MNRAS, 340, 632 (L03)
 Linford J.D., Taylor G.B., Romani R.W., Healey S.E., et al., 2011, ApJ, 726, 16
 Linford J.D., Taylor G.B., Romani R.W., Helmboldt J.F., Readhead A.C.S., Reeves R., & Richards J.L., 2012, ApJ, 744, 177
 Lister M.L., et al. 2009, ApJ. 696, L22
 Liu Y., Jiang D. R., & Gu M. F., 2006, ApJ, 637, 669 (L06)
 Machalski J. & Jamrozy M., 2006, A&A, 454, 95
 Maraschi L., & Tavecchio F., 2003, ApJ, 593, 667
 McLure R.J., & Dunlop J.S., 2001, MNRAS, 327, 199
 Meyer E.T., Fossati G., Georgopoulos M., & Lister M.L., 2011, MNRAS, 740, 98
 Meier D., Koide S., & Uchida Y., 2001, Science, 291, 84
 Meier D.L., 1999, ApJ, 522, 753
 Murphy D.W., Browne I.W.A., & Perley R.A., 1993, MNRAS, 264, 298 (M93)
 Orr, M. J. L., & Browne, I.W. A. 1982, MNRAS, 200, 1067
 Padovani P., 1992, A&A, 256, 399
 Pushkarev, A. B., Kovalev, Y. Y., Lister, M. L., & Savolainen, T. 2012, A&A, 544, 3p
 Pushkarev, A.B., et al. 2009, A&A, 507, L33
 Rawlings S., & Saunders R., 1991, Nature, 349, 138
 Savolainen, T., et al., 2010, A&A, 512, A24

- Sbarrato T., Padovani P., & Ghisellini G., 2014, MNRAS, 445, 81
- Sbarrato T., Ghisellini G., Maraschi L., & Colpi M., 2012, MNRAS, 421, 1764 (Sb12)
- Scarpa R., & Falomo R., 1997, A&A, 325, 109
- Serjeant S., Rawlings S. & Maddox S.J., 1998, MNRAS, 294, 494
- Shaw M. S. et al., 2012, ApJ, 748, 49 (Sh12)
- Shen Y. et al., 2011, ApJS, 194, 45 (S11)
- Tornikoski M., et al. 2010, A&A, 715, 362
- Tremaine S., et al., 2002, ApJ, 574, 740
- Urry C. M., & Padovani P., 1995, PASP, 107, 803
- Wang J. M., Luo B., & Ho L. C., 2004, ApJ, 615, L9 (W04)
- Wang J.M., 2002, ApJ, 579, 554 (WS02)
- Willott C.J., Rawlings S., Blundell K.M., & Lacy M., 1999, MNRAS, 309, 1017
- Woo J. H., & Urry C. M., 2002, ApJ, 579, 530 (W02)
- Wu Z.Z., Gu M.F., & Jiang D.R., 2008, ChJAA, arXiv: 0804.1180v (W08)
- Xie G. Z., Zhou S. B., & Liang E. W., 2004, AJ, 127, 53
- Xie G.Z. et al., 2006, AJ, 131, 1210
- Xie G.Z., Dai H., & Zhou S.B., 2007, AJ, 134, 1464 (X07)
- Xiong D.R., & Zhang X., 2014, MNRAS, 441, 3375
- Xu Y.D., Cao X.W., & Wu Q.W., 2009, ApJ, 694, L107 (X09)
- Yee H.K.C., & Oke J.B., 1978, ApJ, 226, 753
- Zhang J., Liang E. W., Zhang S. N., & Bai J. M., 2012, ApJ, 752, 157 (Z12)
- Zhang J., Sun X.N., Liang E.W., et al., 2014, ApJ, 788, 104
- Zhou M., & Cao X., 2009, RA&A, 9, 293 (Z09)

This paper has been typeset from a Te_X/ L^AT_EX file prepared by the author.

Table 2. The sample of Fermi blazars.

2FGL name (1)	Class (2)	Redshift (3)	Score (4)	Sext (5)	Ref (6)	log M (7)	Ref (8)	log LBLR (9)	Ref (10)
2FGL J0050.6-0929	BZB	0.2	0.57	139.7	K10				
2FGL J0108.6+0135	BZQ	2.099	2.81	530.6	K10	8.83	Z09	46.13,46.98	C99,C97
2FGL J0112.1+2245	BZB	0.265	0.36	3.9	K10				
2FGL J0116.0-1134	BZQ	0.67				8.57,8.92	Sh12	44.62,44.88	Sh12
2FGL J0120.4-2700	BZB	0.559		168	CB99	9.54	X09		
2FGL J0136.9+4751	BZQ	0.859	1.88	8.7	K10	8.73čn8.3čn8.3	W02čnZ09čnC12	44.44	C99
2FGL J0137.6?2430	BZQ	0.835				9.11čn9.13	L06čnW02	45.34	C99
2FGL J0141.5-0928	BZB	0.733		50	CB99	9.84	X09		
2FGL J0205.4+3211	BZQ	1.466	0.65	11.7	K10				
2FGL J0217.9+0143	BZQ	1.715	0.45	71.1	K10				
2FGL J0222.6+4302	BZB	0.444	0.814	1052	A85	8.6	C12		
2FGL J0237.8+2846	BZQ	1.213	2.33	99.9	K10	9.22	Sh12	45.24,45.39,45.9	C99,Sh12,C97
2FGL J0238.7+1637	BZB	0.94	1.51	25.5	K10	9.10,22	Sb12,C12	43.92	C99
2FGL J0252.7?2218	BZQ	1.419				9.4	Sh12	44.73	Sh12
2FGL J0259.5+0740	BZQ	0.893	0.552	39	M93			43.5	C99
2FGL J0315.8?1024	BZQ	1.565				8.33	Sh12	44.67	Sh12
2FGL J0339.4-0144	BZQ	0.852	2.92	70.3	K10	8.89,8.98,8.78	L06,W02čnZ09	45.23,45	C97,L06
2FGL J0405.8-1309	BZQ	0.571	4.33	9.1	K10	9.08,9.07	L06,W02	45.25	L06
2FGL J0423.2-0120	BZQ	0.916	2.91	70.2	K10	9.03čn8.41	W02čnL06	45.59,44.9	C97,C99
2FGL J0424.7+0034	BZB	0.31	1.09	6.1	K10				
2FGL J0428.6-3756	BZB	1.11		86	CB99	8.6	Sb12	44.04	Sb12
2FGL J0442.7?0017	BZQ	0.844				8.81	C12	44.81	Sh12
2FGL J0449.4-4350	BZB	0.107	0.0993	183.2	L08				
2FGL J0453.1-2807	BZQ	2.559						46.26	C99
2FGL J0501.2-0155	BZQ	2.286	1.66	148.1	K10	9.27,8.66	Z09,C12	45.3	C99
2FGL J0530.8+1333	BZQ	2.06	2.24	60.1	K10				
2FGL J0532.7+0733	BZQ	1.254	1.54	126.8	K10	8.43	Sh12	44.86	Sh12
2FGL J0538.8-4405	BZB	0.894		220	CB99	8.8,8.33	Sb12,L06	45.02,44.84	C99,Sh12
2FGL J0608.0-0836	BZQ	0.872	1.2	123.9	K10	8.43,8.825	Z09,Sh12	44.60,45.33	C99,Sh12
2FGL J0635.5-7516	BZQ	0.653				9.41	W02	45.7	C99
2FGL J0654.2+4514	BZQ	0.928				8.17	Sh12	44.26	Sh12
2FGL J0654.5+5043	BZQ	1.253				8.79,7.86	Sh12	43.97	Sh12
2FGL J0710.5+5908	BZB	0.125	0.065	95	GM04	8.26	W02		
2FGL J0710.8+4733	BZB	1.292	0.973	94	M93				
2FGL J0721.9+7120	BZB	0.3	0.69	376.4	K10	8.1	C12		
2FGL J0733.9+5023	BZQ	0.72	0.69	82.5	K10	8.84	Z09		
2FGL J0738.0+1742	BZB	0.424	1.91	20.4	K10	8.4	L03		
2FGL J0739.2+0138	BZQ	0.189	2.34	40.9	K10	8.8,47,7.86	W02,C12,L06	44.19	C99
2FGL J0747.7+4501	BZQ	0.192	0.795	33.09	C04	8.54	S11	44.34	S11
2FGL J0750.6+1230	BZQ	0.889	1.43	27	K10	8.15	L06	44.95	L06
2FGL J0757.1+0957	BZB	0.266	2.07	6.7	K10				
2FGL J0808.2-0750	BZQ	1.837	1.58	59.8	K10				
2FGL J0809.8+5218	BZB	0.138	0.184	4.26	C04	8.9	Z12		
2FGL J0811.4+0149	BZB	1.148	0.46	18.2	K10	8.5	Sb12	43.62	Sb12
2FGL J0816.5+5739	BZB	0.054	0.14	31.2	C04				
2FGL J0825.9+0308	BZB	0.506	1.32	4.1	K10	8.83	C12	43.64,43.37	C97,C99
2FGL J0830.5+2407	BZQ	0.941	0.76	62.7	K10	9.01,9.8,8.7	Sb12,C12,Sh12	44.99,44.97	Sb12,Sh12
2FGL J0831.9+0429	BZB	0.174	0.8	150.8	K10	8.8,8.46	Sb12,C12	42.57	Sb12
2FGL J0834.3+4221	BZQ	0.249				9.68	S11	43.07	S11
2FGL J0841.6+7052	BZQ	2.172	3.34	73.6	K10	9.49čn9.36	Z09čnL06	45.91,46.43	C97,L06
2FGL J0854.8+2005	BZB	0.306	1.57	10.7	K10	8.8,8.79	Sb12,C12	43.58,42.83	C99,Sb12
2FGL J0903.4+4651	BZQ	1.465	1.645	317	M93	9.25	S11	45.26	S11
2FGL J0909.1+0121	BZQ	1.025	1	38	K10	9.32,8.55,9.14	Sb12,L06,Sh12	45.1,45.24,45.27	C99,Sh12,Sb12
2FGL J0915.8+2932	BZB	0.101	0.222	111	A85				
2FGL J0917.0+3900	BZQ	1.267				8.62	S11	44.8	S11
2FGL J0920.9+4441	BZQ	2.19				9.25,9.31,9.29	Sb12,C12,Sh12	45.85,45.7	Sb12,Sh12
2FGL J0921.9+6216	BZQ	1.446	1.11	6.4	K10	8.93	Sh12	45.05	Sh12
2FGL J0927.9-2041	BZQ	0.347				8.46	W02		
2FGL J0929.5+5009	BZB	0.37	0.496	7.94	C04				

Table 2 – continued .

2FGL name (1)	Class (2)	Redshift (3)	S _{core} (4)	S _{ext} (5)	Ref (6)	log M (7)	Ref (8)	log L _{BLR} (9)	Ref (10)
2FGL J0945.9+5751	BZB	0.229	0.069	9.01	C04	8.57,8.77	L11		
2FGL J0948.8+4040	BZQ	1.249	1.23	95	K10	8.95	S11	45.5	S11
2FGL J0956.9+2516	BZQ	0.707	0.483	19	M93	9.34,9.8,7,8.47	Sb12,W02,L06,Sh12	44.92,44.93	C99,Sh12
2FGL J0957.7+5522	BZQ	0.899	2.568	381	M93	8.96,7.87,8.07,8.45	Sb12,L06,W02,Sh12	44.57,44.59	Sb12,Sh12
2FGL J0958.6+6533	BZB	0.368		34	CB99	8.53	C12	42.63	C12
2FGL J1012.5+4227	BZB	0.364	0.07	10	C04		Z12		
2FGL J1015.1+4925	BZB	0.212	0.39	12.31	C04	8.3	S11	44.89	S11
2FGL J1014.1+2306	BZQ	0.566				8.479,8.54	Sh12	45.34	Sh12
2FGL J1017.0+3531	BZQ	1.228				9.1			
2FGL J1019.0+5915	BZB	2.025	0.074	10.4	C04				
2FGL J1031.0+5053	BZB	0.36	0.038	1.25	C04				
2FGL J1033.2+4117	BZQ	1.117				8.65,8.61	Sb12,Sh12	44.93,44.92	Sb12,Sh12
2FGL J1037.6+5712	BZB	0.83	0.128	2.18	C04				
2FGL J1040.7+0614	BZQ	1.27	1.49	11	K10	8.76	Z09		
2FGL J1053.6+4928	BZB	0.14	0.052	16.6	C04				
2FGL J1058.4+0133	BZB	0.888	2.7	230.8	K10	8.45,8.37	Z09,Sh12	44.51,44.52	C99,Sh12
2FGL J1058.6+5628	BZB	0.144	0.208	13.42	C04	8.54	F08		
2FGL J1104.4+3812	BZB	0.03	0.52	181	A85	8.5,8.29,8.22,	Sb12,W02,C12	41.7	Sb12
2FGL J1121.0+4211	BZB	0.124	0.025	0.46	C04				
2FGL J1126.6-1856	BZQ	1.05	0.66	12.4	K10				
2FGL J1130.3-1448	BZQ	1.184	4.58	59.3	K10	9.18	C12	45.77	C12
2FGL J1136.3+6736	BZB	0.134	0.04	10.7	C04				
2FGL J1136.7+7009	BZB	0.046	0.136	217.4	C04	8.21	W02		
2FGL J1143.1+6119	BZB	0.475	0.066	3.52	C04				
2FGL J1146.8-3812	BZB	1.048		10	CB99	8.5	Sb12	44.36,44.60	C99,Sb12
2FGL J1146.9+4000	BZQ	1.089				8.98,8.93	Sb12,Sh12	45.07,45.06	Sb12,Sh12
2FGL J1150.1+2419	BZB	0.2	0.664	25	L08				
2FGL J1151.5+5857	BZB	0.118	0.137	55.2	C04				
2FGL J1159.5+2914	BZQ	0.725	1.55	196.1	K10	9.18,8.54,8.375	Sb12,L06,Sh12	44.71,44.65	Sb12,Sh12
2FGL J1203.2+6030	BZB	0.066	0.157	87.4	C04				
2FGL J1206.0-2638	BZQ	0.786				8.59,9	L06,W02	44.07	L06
2FGL J1209.6+4121	BZB	0.377	0.397	1.18	C04				
2FGL J1217.8+3006	BZB	0.13	0.355	189	A85	8.12	W02		
2FGL J1219.7+0201	BZQ	0.24				8.87	S11	44.83	S11
2FGL J1221.3+3010	BZB	0.182	0.067	4.3	GM04	8.6	Z12		
2FGL J1221.4+2814	BZB	0.102	2.058	2.2	A85	7.8	C12	42.25	C12
2FGL J1222.4+0413	BZQ	0.966	0.6	155.5	K10	8.24,8.37	Sb12,Sh12	44.86,44.97	Sb12,Sh12
2FGL J1224.9+2122	BZQ	0.432	1.1	956.4	K10	8.87,8.44,8.9	Sb12,C12,Sh12	45.21,45.16	Sb12,Sh12
2FGL J1229.1+0202	BZQ	0.158	34.89	17671	K10	8.9,7.22,8.92	Sb12,W02,L06	45.54,45.53,45.82	C99,Sb12,C97
2FGL J1243.1+3627	BZB	1.065	0.115	32.6	C04				
2FGL J1246.7?2546	BZQ	0.633				9.04	W02		
2FGL J1248.2+5820	BZB	0.847	0.18	4.2	C04				
2FGL J1253.1+5302	BZB	0.445	0.378	42.05	C04				
2FGL J1256.1-0547	BZQ	0.536	10.56	2095	K10	8.9,8.43,8.28	Sb12,W02,L06	44.61,44.38	C99,Sb12
2FGL J1309.4+4304	BZB	0.69	0.055	2.87	C04				
2FGL J1310.6+3222	BZB	0.998	1.33	69.1	K10	8.8,9.24,8.57	Sb12,C12,Sh12	45.09,44.92,44.92	C99,Sh12,Sb12
2FGL J1317.9+3426	BZQ	1.056				9.29,9.14	Sb12	45.07,45.09	Sh12
2FGL J1326.8+2210	BZQ	1.4	1.14	20.4	K10	9.24,9.25	Sb12,Sh12	44.90,44.96	Sb12,Sh12
2FGL J1337.7-1257	BZQ	0.539	2.07	151	K10	7.98	L06	44.43,44.18	C97,L06
2FGL J1354.7?1047	BZQ	0.332				8.15	W02		
2FGL J1419.4+3820	BZQ	1.82	0.52	2.5	K10	8.59,8.68	S11	45.1	S11
2FGL J1420.2+5422	BZB	0.153	1.058	18	A85	8.74	W08	43.27	X07
2FGL J1428.0?4206	BZQ	1.522				9.7	L03	44.95	C99
2FGL J1428.6+4240	BZB	0.129	0.032	29.3	GM04	9.13	W02		
2FGL J1439.2+3932	BZB	0.344				8.95	W08		
2FGL J1442.7+1159	BZB	0.163	0.06	8.5	GM04				
2FGL J1504.3+1029	BZQ	1.839	1.82	38.3	K10	9.64,8.74,8.94	Sb12,L06,Sh12	45.30,45.17	Sb12,Sh12
2FGL J1510.9?0545	BZQ	1.185				8.97	C12	45.52	C12
2FGL J1512.2+0201	BZQ	0.219				8.84,7.99	Sb12,W02	43.02	Sb12
2FGL J1512.8-0906	BZQ	0.36	1.45	180.2	K10	8.6,8.65,8.2	Sb12,W02,L06	44.75	C99

Table 2 – continued .

2FGL name (1)	Class (2)	Redshift (3)	S _{core} (4)	S _{ext} (5)	Ref (6)	log M (7)	Ref (8)	log L _{BLR} (9)	Ref (10)
2FGL J1516.9+1925	BZB	1.07	0.255	1.7	A85				
2FGL J1517.7-2421	BZB	0.049	2.562	32	A85	8.1	W02	41.75	X07
2FGL J1540.4+1438	BZB	0.605	1.67	71.4	K10	8.94	W04	43.36,43.05	C97,W04
2FGL J1542.9+6129	BZB	0.117	0.126	3.7	C04				
2FGL J1549.5+0237	BZQ	0.414	1.15	18.8	K10	8.61,8.72,8.47,8.67	Sb12,W02,L06,Sh12	44.67,44.83,44.91	C99,Sh12,Sb12
2FGL J1550.7+0526	BZQ	1.422	2.21	42.9	K10	9.38,8.98	Sb12,Sh12	45.06,45.08	Sb12,Sh12
2FGL J1553.5+1255	BZQ	1.29				9.1,8.64	Sh12	45.20,45.18	Sh12
2FGL J1559.0+5627	BZB	0.3	0.181	19.7	C04				
2FGL J1607.0+1552	BZB	0.497				8.58	F08		
2FGL J1608.5+1029	BZQ	1.226	1.35	26.5	K10	8.64,9.5,8.77	Sb12,C12,Sh12	45.01,45.07	Sb12,Sh12
2FGL J1613.4+3409	BZQ	1.399	2.83	20.6	K10	9.12,9.57,9.6,9.08	Sb12,W02,L06,Sh12	45.87,45.46,45.50	C99,Sh12,Sb12
2FGL J1635.2+3810	BZQ	1.813	2.17	32	K10	9.53,9.67,9.075	Sb12,C12,Sh12	45.82,45.67,45.76	C99,Sh12,Sb12
2FGL J1637.7+4714	BZQ	0.74				8.61,8.52	Sh12	44.58	Sh12
2FGL J1640.7+3945	BZQ	1.66	1.17	27.6	K10	8.5	D03	45.88	C99
2FGL J1653.9+3945	BZB	0.0337	1.376	67	A85	9.9,21	Sb12,W02	42.2	Sb12
2FGL J1719.3+1744	BZB	0.137	0.661	11	A85				
2FGL J1725.2+5853	BZB	0.297	0.052	20.4	C04				
2FGL J1728.2+0429	BZQ	0.296				8.07,7.72	W02,L06	44.07	C99
2FGL J1727.1+4531	BZQ	0.717	1	55.3	K10	8.22	W02		
2FGL J1728.2+5015	BZB	0.055	0.175	50	A85	7.86	W02		
2FGL J1731.3+3718	BZB	0.204	0.062	40.09	C04				
2FGL J1733.1-1307	BZQ	0.902	6.13	517.8	K10	9.3	C12	44.83	C12
2FGL J1740.2+5212	BZQ	1.375	1.61	27.6	K10	9.32	L06	45.16	L06
2FGL J1742.1+5948	BZB	0.4	0.106	5	C04				
2FGL J1749.1+4323	BZB	0.215	0.235	19.5	C04				
2FGL J1751.5+0938	BZB	0.322	1.05	4.9	K10	8.7,8.34	Sb12,C12	43.7	Sb12
2FGL J1748.8+7006	BZB	0.77		12	CB99			44.87	WS02
2FGL J1801.7+4405	BZQ	0.663	0.5	246.6	K10				
2FGL J1800.5+7829	BZB	0.684	1.98	20.8	K10	8.6,7.92	Sb12,L06	44.85	Sb12
2FGL J1806.7+6948	BZB	0.051	1.2	368.7	K10	8.7,8.51	Sb12,W02	42	Sb12
2FGL J1824.0+5650	BZB	0.664	0.95	137.4	K10	9.26	C12	43.32	C12
2FGL J1838.7+4759	BZB	0.3	0.051	1.2	C04				
2FGL J1849.4+6706	BZQ	0.657	0.47	101	K10	9.14	W02	46.2	C99
2FGL J2000.8-1751	BZQ	0.65	1.82	9.4	K10			44.42	C97
2FGL J2000.0+6509	BZB	0.047	0.2	60	GM04	8.09	W02		
2FGL J2004.5+7754	BZB	0.342	0.823	28.9	M93	8.8	G11	43.48	X07
2FGL J2025.6-0736	BZQ	1.388				9.7	L03		
2FGL J2035.4+1058	BZQ	0.601	0.781	40	A85	7.74,8.26	Sh12	44.17	Sh12
2FGL J2133.8-0154	BZQ	1.285	1.37	151.9	K10			43.66	C12
2FGL J2143.5+1743	BZQ	0.211				8.6,8.74	Sb12,W02	44.26	Sb12
2FGL J2147.3+0930	BZQ	1.113	0.698	82	M93				
2FGL J2148.2+0659	BZQ	0.99	2.87	27.7	K10	8.87	L06	46.24,45.77	C97,C99
2FGL J2157.9-1501	BZQ	0.672	2.7	304.7	K10	7.59	W02	43.68	C99
2FGL J2158.8-3013	BZB	0.117	0.252	132	A85	8.7	Z12		
2FGL J2202.8+4216	BZB	0.069	1.99	14.2	K10	8.7,8.23	Sb12,W02	42.52	Sb12
2FGL J2204.6+0442	BZB	0.027	0.179	656	GM04	8.1	W02		
2FGL J2203.4+1726	BZQ	1.075	0.87	74.6	K10				
2FGL J2211.9+2355	BZQ	1.125	0.43	0.9	K10	8.46	Sh12	44.78	Sh12
2FGL J2225.6-0454	BZQ	1.404	7.13	91.6	K10	8.81,8.54	W04,C12	45.6	C99
2FGL J2229.7-0832	BZQ	1.56	0.93	8.4	K10	8.95,8.62	Sb12,Sh12	45.66,45.45	Sb12,Sh12
2FGL J2232.4+1143	BZQ	1.037	6.99	148	K10	8.7,8.64	Sb12,C12	45.87,45.62	C99,Sb12
2FGL J2236.4+2828	BZQ	0.795	1.118	3.4	M93	8.35	Sh12	44.37	Sh12
2FGL J2243.2-2540	BZB	0.774				8.6	Sb12	43.5,43.46	C99,Sb12
2FGL J2253.9+1609	BZQ	0.859	14.09	822	K10	8.7,9.17,8.83	Sb12,W02,L06	45.65,45.52	C99,Sb12
2FGL J2258.0-2759	BZQ	0.927				8.92,9.16	L06,W02	45.84	L06
2FGL J2334.3+0734	BZQ	0.401	0.61	38.4	K10	8.37	Sh12	44.93	Sh12
2FGL J2347.9-1629	BZQ	0.576	1.99	142.7	K10	8.72,8.47	W02,L06	44.62,44.36	C97,C99
2FGL J2359.0-3037	BZB	0.165	0.039	27.2	GM04	8.6	W02		

Table 3. The sample of non-Fermi blazars.

Name (1)	Class (2)	Redshift (3)	Score (4)	Sext (5)	Ref (6)	log M (7)	Ref (8)	log L _{BLR} (9)	Ref (10)
PKS 0003-066	BZQ	0.347	2.66	43.9	K10			43.12	C99
0007+106	BZQ	0.0893	0.08	17.6	K10		C12	44.14	C12
0016+731	BZQ	1.781	0.4	7.8	K10	8.93	Z09	44.98	C12
0119+115	BZQ	0.57	1.24	113.7	K10				
1ES 0145+138	BZB	0.125	0.003	32.8	GM04	8.42	W02		
0146+056	BZQ	2.345	0.865	42	M93				
0149+218	BZQ	1.32	1.089	25	M93				
0221+067	BZQ	0.511				7.29	W02		
0224+671	BZQ	0.523	1.48	149.2	K10				
0229+131	BZQ	2.059	1.118	212	M93			46.61,45.98	C97,C99
IERS B0229+200	BZB	0.14	0.042	52.2	GM04	9.24	W02		
1ES 0347-121	BZB	0.185	0.009	16.7	GM04	8.65	W02		
0350-371	BZB	0.165	0.023	17.1	GM04	8.82	W02		
0400+258	BZQ	2.109	1.382	1.3	M93			46.58	C99
TXS 0446+113	BZQ	1.375	1.56	15.4	K10	9.44	S12	44.49	S12
0548-322	BZB	0.069	0.08	218	A85	8.15	Z12		
0607-157	BZQ	0.323	3.02	1.1	K10	9.162	G01	43.56	C12
0642+449	BZQ	3.396	0.65	1.4	K10			48.66	C99
B3 0707+424	BZQ	1.163	0.267	33.37	C04				
0711+356	BZQ	1.62	1.543	4.2	M93			47.06	C99
TXS 0724+571	BZQ	0.426	0.437	25.64	C04				
IERS B0730+353	BZB	0.177	0.046	56.74	C04				
0731+479	BZQ	0.782	0.357	47.96	C04				
0738+313	BZQ	0.632	2.16	65	K10	9.57	L06	45.78	L06
0742+103	BZQ	2.624	3.62	5.8	K10				
PKS 0745+241	BZQ	0.409	0.719	196	M93	7.92	C12		
IERS B0756+503	BZQ	1.622	0.114	4.23	C04	9.52	S11	45.66	S11
0812+367	BZQ	1.027				9.2	S11	45.29	S11
0818-128	BZB	0.074	0.63	375	A85				
SBS 0818+506	BZQ	2.133	0.053	0.83	C04	9.71	S11	45.83	S11
PKS 0820+22	BZB	0.951	0.161	602.5	M93	9.5435	X09	44.16	C99
0828+493	BZB	0.548		0.025	CB99	9.01	X09		
0833+585	BZQ	2.101	0.678	30	M93	9.8	S11	45.79	S11
0836+182	BZB	0.28	0.31	88.3	L08				
0839+187	BZQ	1.276	1.264	7	M93	9.79	S11	45.73	S11
B3 0840+378	BZQ	1.731	0.062	4.61	C04	9.48	S11	45.42	S11
HS 0846+5942	BZQ	1.71	0.012	1.51	C04	9.65	S11	46.28	S11
IERS B0850+536	BZQ	2.422	0.021	0.73	C04	9.95	S11	45.97	S11
0850+581	BZQ	1.319				8.49	L06	45.66	L06
IERS B0850+625	BZB	0.267	0.278	9.75	C04				
0923+392	BZQ	0.695	2.83	361.8	K10	9.756,9.4	G01,W04	46.06,45.23	C97,W04
1ES 0927+500	BZB	0.187	0.021	1.3	GM04	8.34	W02		
SBS 0949+510	BZQ	1.09	0.105	5.51	C04	9.35	S11	45.12	S11
0955+476	BZQ	1.882	0.62	1.1	K10	9.56	S11	45.27	S11
1022+194	BZQ	0.828				8.9	S11	45.26	S11
IERS B1032+382	BZQ	1.51	0.053	1.5	C04	9.73	S11	45.57	S11
GB6 J1033+4222	BZB	0.211	0.026	7.19	C04				
1036+054	BZQ	0.473	0.94	57	K10				
1045-188	BZQ	0.595	0.76	509.4	K10	7.308	G01	43.8	C99
GB6 J1049+3737	BZQ	2.997	0.055	1.07	C04			45.87	S11
IERS B1051+391	BZQ	1.372	0.072	1.01	C04	9.54	S11	45.22	S11
1055+201	BZQ	1.11	0.768	1826	M93	9.42	S11	45.8	S11
TXS 1059+599	BZQ	1.83	0.416	3.04	C04				
TXS 1108+527	BZQ	1.285	0.04	76.17	C04	9.4	S11	45.23	S11
1116+128	BZQ	2.126	1.888	259	M93	8.88	S11	45.67	S11
SBS 1116+603	BZQ	2.641	0.186	5.55	C04	9.79	S11	46.36	S11
IERS B1121+518	BZB	0.235	0.044	5.99	C04				
B3 1128+385	BZQ	1.74	0.869	5.4	M93	9.29	C12	46.26	C12
GB6 J1140+4622	BZQ	0.114	0.079	2.72	C04	8.09	S11	43.77	S11
BWE 1145+5710	BZQ	0.451				8.88	S11	44.8	S11

Table 3 – continued .

Name (1)	Class (2)	Redshift (3)	S _{core} (4)	S _{ext} (5)	Ref (6)	log M (7)	Ref (8)	log L _{BLR} (9)	Ref (10)
IERS B1146+531	BZQ	1.638	0.096	4.86	C04	9.51	S11	45.92	S11
SBS 1149+499	BZQ	1.094				9.26	S11	45.52	S11
1150+812	BZQ	1.25	1.89	89.2	K10				
1150+497	BZQ	0.334	0.6	1100	A85	8.45	L06	44.39	L06
B3 1159+450	BZB	0.297	0.047	59.03	C04				
IERS B1200+483	BZQ	0.816	0.067	1.7	C04	9.47	S11	45.42	S11
IERS B1201+454	BZQ	1.075	0.032	1.71	C04	9.19	S11	45.38	S11
IERS B1212+078	BZB	0.136	0.085	65	GM04	8.99	W02		
B3 1212+467	BZQ	0.72	0.161	117.41	C04	9.09	S11	45.12	S11
SBS 1215+521	BZQ	2.229	0.079	2.16	C04	9.14	S11	46.27	S11
SBS 1221+503	BZQ	1.064	0.044	1.78	C04	9.14	S11	45.18	S11
1229+645	BZB	0.163	0.055	8	GM04	9.41	W02	43.04	WS02
TXS 1231+481	BZQ	0.372	0.352	10.05	C04	8.26	S11	44.8	S11
BZQ J1235+5228	BZQ	1.653	0.082	1.78	C04	9.59	S11	45.5	S11
1ES 1255+244	BZB	0.141	0.0065	10.1	GM04	8.58	W02		
BZB J1301+4416	BZB	0.435	0.052	2.11	C04				
1309+355	BZQ	0.183	0.044	0.8	C04	8.8	S11	44.51	S11
1347+539	BZQ	0.98	0.96	87.96	C04	9.43	S11	45.31	S11
IERS B1354+418	BZQ	0.697	0.023	0.84	C04				
BWE 1413+4844	BZB	0.496	0.043	0.82	C04				
1354+195	BZQ	0.72	1.309	855	M93	9.44	W02	46.43	C99
1400+162	BZB	0.244	0.233	548	A85			42.27	C97
1402+044	BZQ	3.209				8.94	S11	46.07	S11
B3 1409+429	BZQ	0.887	0.071	1.14	C04	9.51	S11	45.26	S11
IERS B1411+746	BZB	0.46	0.113	15	C04				
IERS B1413+487	BZB	0.496	0.043	0.82	C04				
SBS 1421+511	BZQ	0.276	0.118	21.14	C04	7.57	S11	44.17	S11
B3 1429+401	BZQ	1.217	0.208	2.17	C04	9.96	S11	45.82	S11
1435+638	BZQ	2.068	0.86	22.41	C04	9.43	S11	46.05	S11
1504-166	BZQ	0.876	2.39	11.4	K10	8.84	Z09	45.57	C99
1522+155	BZQ	0.628	0.335	68	A85	8.47	S11	44.7	S11
SBS 1550+582	BZQ	1.324	0.192	8.62	C04				
1602+576	BZQ	2.85	0.333	9.2	C04				
B2 1604+27	BZQ	0.934				8.83	S11	44.91	S11
IERS B1612+378	BZQ	1.53	0.049	1.85	C04	9.68	S11	45.75	S11
SBS 1618+530	BZQ	2.347	0.179	5.69	C04				
1621+392	BZQ	1.981	0.19	2.89	C04	9.67	S11	46.01	S11
1637+574	BZQ	0.751	1.01	71.4	K10	9.18,9.22	W02,L06	45.57	L06
1641+399	BZQ	0.593	7.95	1476.9	K10	9.03čn9.27	Z09čnL06	45.47	L06
B3 1642+458	BZB	0.225	0.105	78.97	C04				
1642+690	BZQ	0.751	0.999	330	M93	7.76	W02	46.15	C99
IERS B1649+401	BZQ	2.342	0.043	1.17	C04	9.12	S11	46.38	S11
1655+077	BZQ	0.621	1.27	199.1	K10	7.91	Z09	43.62	C12
1656+053	BZQ	0.879	1.301	96	M93	9.09čn9.74	Z09čnL06	46.26	L06
1656+571	BZQ	1.281	0.814	158.62	C04				
B3 1659+399	BZB	0.507	0.251	3.95	C04				
IERS B1705+717	BZB	0.35	0.0384	1.8	C04				
1718+481	BZQ	1.084	0.061	1.08	C04				
IERS B1726+552	BZQ	0.247	0.142	7.34	C04				
1727+386	BZQ	1.39	0.24	5.14	C04				
1741-038	BZQ	1.054	1.7	3.5	K10	9.3	L03	46.77	C99
1751+288	BZQ	1.115	0.27	8.1	K10				
1758+388	BZQ	2.092	0.33	3.2	K10				
1928+738	BZQ	0.302	3.22	356.5	K10	8.72	W04	44.61	W04
1936-155	BZQ	1.657	1.08	10.5	K10	9.3	L03		
2005+403	BZQ	1.736	2.47	10.6	K10				
2008-159	BZQ	1.18	0.55	7.5	K10	9.56	Z09		
IERS B2021+614	BZQ	0.227	2.67	1.3	K10				
2037+511	BZQ	1.686	4.97	657.6	K10				

Table 3 – continued .

Name (1)	Class (2)	Redshift (3)	S _{core} (4)	S _{ext} (5)	Ref (6)	log M (7)	Ref (8)	log L _{BLR} (9)	Ref (10)
2121+053	BZQ	1.941	1.08	4.8	K10	8.6	Z09		
2128-123	BZQ	0.501	1.42	39.8	K10	9.16–9.02	Z09–L06	45.42	L06
2134+004	BZQ	1.944	4.82	6.6	K10	8.91	W04	44.75	W04
2136+141	BZQ	2.427	1.14	0.8	K10			45.63	C99
2142+110	BZQ	0.548				8.69	S11	44.84	S11
2201+315	BZQ	0.295	1.54	378.4	K10	8.91–8.94	Z09–L06	45.46	L06
2216-038	BZQ	0.901	1.76	312.7	K10	9.08	L06	45.79	L06
2223+210	BZQ	1.959	1.766	47	M93			49.817	C99
2243-123	BZQ	0.632	2.27	27.7	K10	8.32	C12	45.28	C12
2254+074	BZB	0.19	0.454	17	A85	8.62	W02	42.82	WS02
PKS 2316-423	BZB	0.054	0.25	391.9	L08				
2328+107	BZQ	1.489	1.065	25	M93			48.14	C99
2344+092	BZQ	0.677	1.801	26	M93	9.31	W02	47.73	C99
2351+456	BZQ	1.992	2.35	6.9	K10	9.22	Z09	45.11	C97